DOI: 10.1002/ejic.201001014

Bond Activation in Iron(II)-Coordinated Polypodal Phosphane Ligands

Simon-Andreas Gentschow,[a] Stephan W. Kohl,[a] Walter Bauer,*[b] Markus Hummert,[a] and Andreas Grohmann*[a]

In memory of Herbert Schumann

Keywords: Bond activation / N,P ligands / Iron / NMR spectroscopy / Phosphane ligands

A mononuclear iron(II) complex is readily formed when combining equimolar amounts of iron(II) tetrafluoroborate hexahydrate, the pyridine-derived triphosphane $C_5H_3N\{2\text{-}[CMe(CH_2PMe_2)_2]\}\{6\text{-}[CMe_2(CH_2PMe_2)]\}$ (**2**) and diethylphosphane (Et_2PH) in methanol at room temperature. The chelate ligand is in fact pentadentate, as one of the methyl groups of the neopentyl-like sidearm engages in a C–H-bonded contact (agostic interaction) with the metal centre, in addition to the expected NP_3 coordination. The remaining site of what is a distorted coordination octahedron is occupied by monodentate Et_2PH. The autoclave reaction of this purple complex with CO (10 bar, ethanol solvent, 65 °C) yields a yellow microcrystalline precipitate, whose analysis reveals a mixture of two products, in an approximate ratio of 40:1. One of the products is the *cis*-dicarbonyl complex $[Fe(\mathbf{2})(CO)_2](BF_4)_2$ (**4**), in which the chelate ligand acts as an NP_3 donor, and the other is the monocarbonyl complex of the tetrapodal pentadentate NP_4 ligand **1**. The latter ligand is formed from **2** by incorporation of an additional PMe_2 donor, in what, in effect, is a metal-mediated phosphenium group transfer. A mechanism is suggested for this reaction. Other species in the reaction mixture have been identified on the basis of mass spectra, and the full NMR spectroscopic assignment of complex **4** (^1H, ^{31}P, ^{13}C) is reported.

Introduction

Tetrapodal pentadentate ligands are a recent addition to the coordination chemist's toolbox.[1] The ligands are designed to occupy five coordination positions in an octahedral complex, thereby providing a single site for the coordination of a small monodentate ligand or substrate. Depending on the nature of the transition metal and the chelate ligand, the substrate is set up for transformation reactions, such as reduction,[2] bond cleavage,[3] metathesis[4] or reductive elimination[5]. In this context, we have been studying the reactivity of iron complexes of the NP_4 ligand **1** and found the ligand to undergo specific P–C bond activation in nucleophilic solvents such as methanol, which results in the cleavage of one ligand arm (Scheme 1).[6–9]

A particularly remarkable finding is that bond scission may be reversed under certain conditions.[6] In an effort to shed light on the mechanism of (re)formation of a P–C bond in the coordination sphere of iron(II), we embarked on a coordination chemical study of the tripodal tetradentate ligand **2** (NP_3, which is the chelate ligand remaining after the breaking of the P–C bond, Scheme 1). The synthesis of the NP_3 ligand (Scheme S1, Supporting Information) starts from 2-ethyl-6-isopropylpyridine and is a sequence of exhaustive hydroxymethylation and nucleophilic substitution reactions.[7]

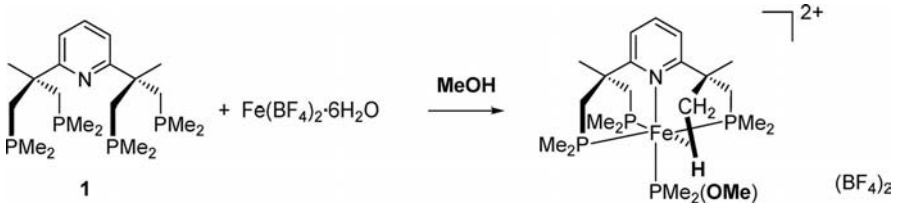

Scheme 1. Solvent-induced P–C bond cleavage in **1** upon complexation to iron(II).

Complex formation of **2** with $Fe(BF_4)_2{\cdot}6H_2O$ and a co-ligand occurs readily. When using methyl diethylphosphin-

[a] Technische Universität Berlin, Institut für Chemie, Strasse des 17. Juni 135, 10623 Berlin, Germany
E-mail: andreas.grohmann@chem.tu-berlin.de
[b] Universität Erlangen-Nürnberg, Department Chemie und Pharmazie, Organische Chemie, Henkestrasse 42, 91054 Erlangen, Germany
E-mail: bauer@chemie.uni-erlangen.de

Supporting information for this article is available on the WWW under http://dx.doi.org/10.1002/ejic.20101014.

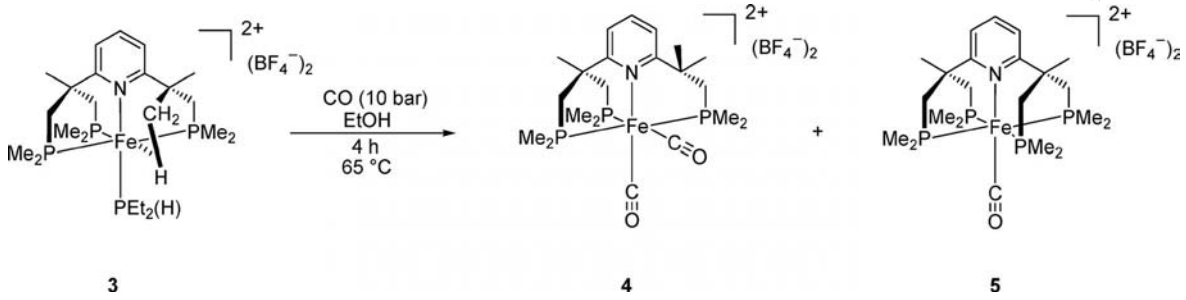

Scheme 2. Product mixture (yellow polycrystalline material) isolated from the reaction of **3** with CO in ethanol. The generation of complex **5** requires specific formation of a P–C bond.

ite, $Et_2P(OMe)$, as coligand, the expected product is formed in which the chelate ligand acts as a tetradentate ligand (one of the methyl groups of the neopentyl monophosphane sidearm is in agostic interaction with the iron ion)[10] and $Et_2P(OMe)$ is monodentate. There is, however, a second, minor product (**3**), which contains diethylphosphane (Et_2PH) as a monodentate ligand.[7] Complex **3**, when reacted with excess CO in an autoclave (ethanol solvent; 4 h, 65 °C) is transformed into a number of products. Two of these have so far been isolated (Scheme 2; the identity of both products has been verified by X-ray crystallography):[7] The first is the result of replacement of the agostic methyl group and the diethylphosphane ligand by two equivalents of CO (complex **4**), and the second is complex **5**, which contains the NP_4 ligand $C_5H_3N[CMe(CH_2PMe_2)_2]_2$ (**1**). This is the very ligand which, in the presence of iron(II) and nucleophilic solvents (such as MeOH, EtOH, H_2O), undergoes specific P–C bond cleavage (Scheme 1).[6] Ligand **1** is now the product of a P–C bond *forming* reaction in the coordination sphere of the iron(II) ion. If, in the reaction at hand, **1** is generated in an *inter*molecular process, a second equivalent of complex **3**, or an intermediate into which it is transformed, is expected to provide the required PMe_2 fragment. We have no indication that the coordinated diethylphosphane ligand in **3** is active in this reaction. The formation of an NP_3P' ligand (three dimethylphosphanyl residues, one diethylphosphanyl group) is not observed. The present contribution reports the direct synthesis of complex **3**, undertakes the complete NMR spectroscopic characterization and assignment (^1H, ^{13}C, ^{31}P) of complex **4**, and suggests a mechanism for the formation of complex **5**, on the basis of mass spectrometric results.

Results and Discussion

The direct synthesis of complex **3**, by the reaction of the NP_3 ligand **2** and diethylphosphane with $Fe(BF_4)_2{\cdot}6H_2O$ in methanol, proceeds as shown in Scheme 3 (60% yield based on **2**).

Complex **3** is obtained as a purple microcrystalline solid. The most significant signal in the ^1H NMR spectrum (Figure S1, Supporting Information) is a very prominent and slightly broadened resonance at high field ($\delta = -3.72$ ppm), which is characteristic of the methyl group in close (agostic) contact with the metal centre. The broadening is due to rotation of the methyl group, which apparently is relatively slow on the NMR timescale. The three protons of the pyridine ring give rise to an ABC spin system (triplet, doublet, doublet) between ca. 7.6 and 8.2 ppm. The region between ca. 0.7 and 2.7 ppm shows the partially overlapping signals assigned to the six PMe_2 groups, the two methyl groups on the quaternary carbon atoms, the three methylene groups and the two ethyl groups of the diethylphosphane ligand. The resonance of the H atom bonded to phosphorus is a broadened doublet at 4.7 ppm with a coupling constant of ca. 330 Hz. The proton-coupled ^{31}P NMR spectrum shows four signals in total. The three signals at ca. 47, 24 and 19 ppm represent the three PMe_2 groups of the coordinated triphosphane **2**, and the signal at ca. 40 ppm belongs to the diethylphosphane ligand. The coupling constant $^1J(P–H)$ is ca. 330 Hz, in keeping with the ^1H NMR result. The integrated intensities of all signals are as expected.

The reaction of complex **3** (as obtained by direct synthesis) with CO (10 bar) in ethanol in an autoclave (4 h, 65 °C) produces a yellow microcrystalline precipitate. Its spectroscopic characterization (^1H, ^{13}C, ^{31}P NMR, IR) confirms

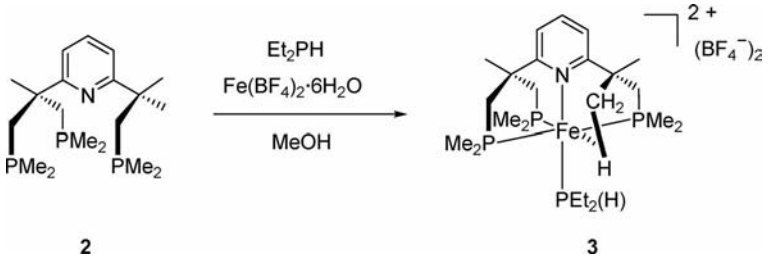

Scheme 3. Direct synthesis of complex **3**.

that the material is a mixture of the complexes **4** and **5** (see Scheme 2). This is especially well illustrated in the ^{31}P NMR spectrum (Figure S2, Supporting Information), which has three prominent signals (for the three PMe_2 groups of the NP_3 ligand **2** of the dicarbonyl complex **4**) and a singlet of lower intensity at δ = 19.26 ppm, for the four equivalent PMe_2 groups of the NP_4 ligand of complex **5**. The latter assignment is in agreement with the ^{31}P chemical shift value (δ =19.00 ppm) determined for an authentic sample of **5**, which had previously been obtained by a different route.[6]

The solid-state IR spectrum of the reaction mixture (KBr disc; Figure S3, Supporting Information) has two strong signals in the diagnostic region,[14,15] at 2060 and 2015 cm^{-1}, which we assign to the symmetric and asymmetric CO stretching modes, respectively, of the *cis*-dicarbonyl complex **4**. The stretching of the CO bond for one carbonyl ligand lowers its π^* orbital energy and thus favours backdonation from the metal ion. Less electron density is now available for backdonation into the second CO ligand, and its CO bond is thus strengthened. Consequently, the simultaneous stretching of two CO bonds in a symmetric fashion requires a greater input of energy than the asymmetric stretching mode.[16] The low-frequency band has a shoulder at 2003 cm^{-1}, which we assume arises from the CO stretching vibration of the monocarbonyl complex **5**. This complex was previously found to contain a strongly distorted NP_4 coordination cap, and a carbonyl band at 1969 cm^{-1} is reported in its spectrum. The ν_{str}(CO) mode is expected to depend sensitively on the overall complex geometry, as enforced by the solid-state matrix.

Mass spectra (ESI) of an acetonitrile solution of the yellow reaction product show four prominent signals for the dication in **4** ($\mathbf{4}^{2+}$, *m*/*z* = 241.564), the fragment [$\mathbf{4}^{2+}$ – CO] (*m*/*z* = 227.567), the fragment [$\mathbf{4}^{2+}$ – 2CO] (*m*/*z* = 213.570) and the acetonitrile adduct [$\mathbf{4}^{2+}$ – 2CO + CH_3CN] (*m*/*z* = 234.083). As is evident from Figure 1, there is excellent agreement between measured and simulated spectra. Two low-intensity signals (at *m*/*z* = 243.576 and 257.574), again matched perfectly by simulation (not shown), are assigned to the dication in **5** ($\mathbf{5}^{2+}$) and the fragment [$\mathbf{5}^{2+}$ – CO], respectively. Finally, elemental analysis of the polycrystal-

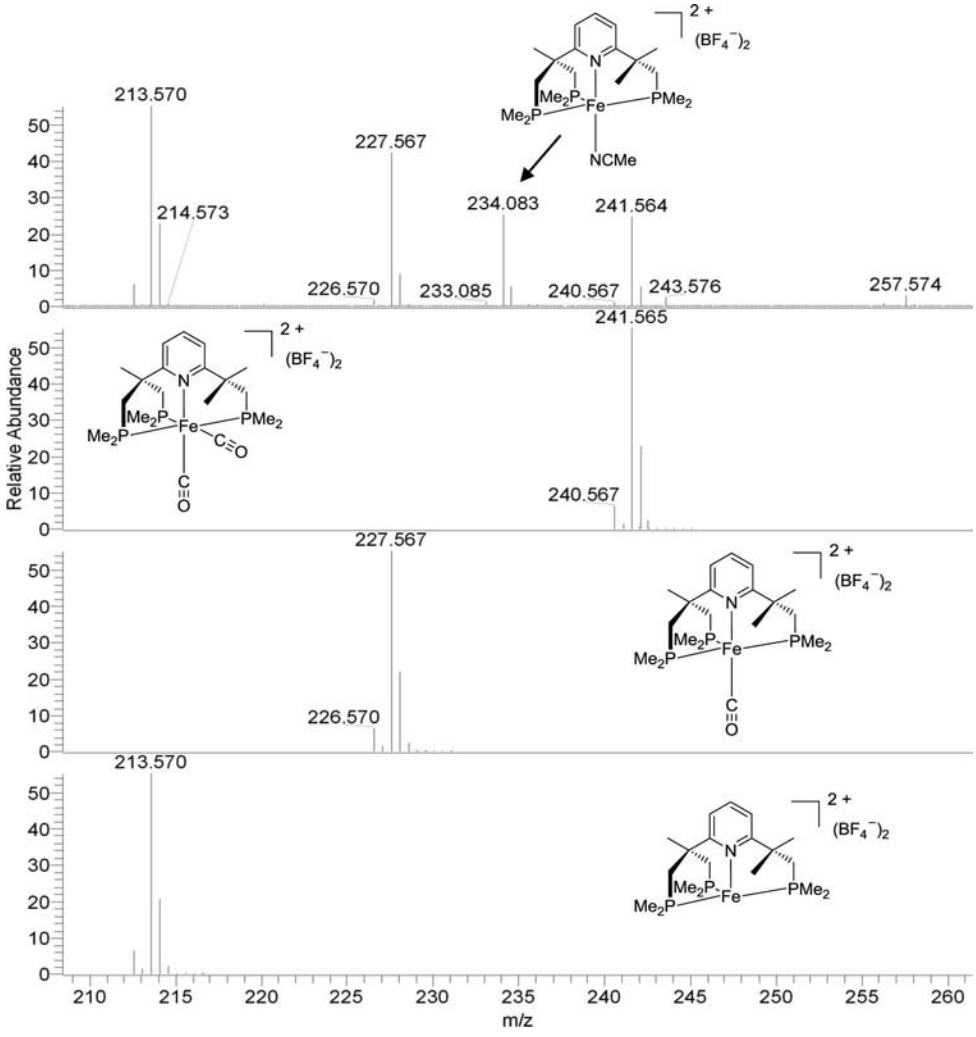

Figure 1. Experimental ESI mass spectrum (top) and simulated spectra (below) of an acetonitrile solution of the yellow product mixture of complexes **4** and **5** (cf. Scheme 2).

line yellow mixture gives CHN values (in %) of 38.76, 5.65 and 2.09, respectively, which are in the range of values calculated for **4** (C 38.40, H 5.52, N 2.13) and **5** (C 38.36, H 6.00, N 2.03).

The complex ion in **4** has quite regular pseudo-octahedral symmetry in the solid state, characterized by bond angles around iron that are close to 90 and 180°.[7] An NMR study, which has achieved the complete "ab initio" assignment of all ^{1}H and ^{31}P signals, indicates that the structure of the dication in solution does not deviate significantly from the solid-state structure. The latter, with the numbering scheme used in the NMR assignment, is given in Figure 2.

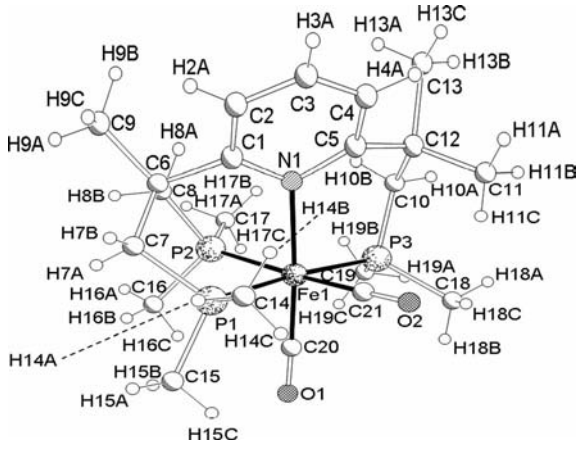

Figure 2. X-ray structure of the dication in complex **4** and the numbering scheme used for the NMR assignment.

The ^{1}H NMR spectrum of **4**, both in the ^{31}P-coupled and ^{31}P-decoupled mode, is shown in Figure 3. The assignment starts from the unique signals of H9, H11 and H13. The H9 signal is split into a triplet because of equally strong coupling with P1 and P2. The three H11 protons show no coupling with P3, owing to a dihedral angle C11–C12–C10–P3 that is close to 90° (Karplus relationship); the angle is

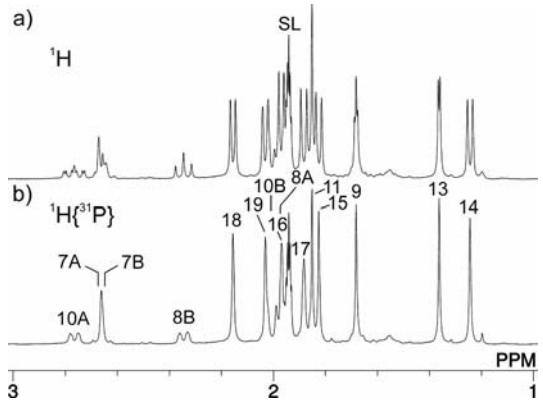

Figure 3. (a) Phosphorus-coupled and (b) phosphorus-decoupled ^{1}H NMR spectrum of **4** (500 MHz, CD_3CN, +25 °C). Only the aliphatic region is shown (for pyridine signals, see Figure S4b, Supporting Information). Numbers refer to the numbering of the X-ray structure shown in Figure 2. For assignments, see text. SL = solvent signal.

67° in the solid-state structure (Figure 2). By contrast, the dihedral angle C13–C12–C10–P3 is 177° (solid state), thus close to the maximum in the Karplus curve. Accordingly, P3 coupling causes the H13 signal to split into a doublet.

Further assignments are based on the $^{1}H,^{1}H$ NOESY spectrum (Figure S4, Supporting Information). The protons H13 have cross-peaks of approximately equal intensity with either of those of the diastereotopic protons H10A and H10B (Figure S4a), consistent with the X-ray structure. The distance H11–H10A is, however, considerably smaller than the distance H11–H10B. This explains why only the H11–H10A cross-peak is found in the NOESY plot, whereas the H11–H10B cross-peak is missing.

Trivially, there is an intense cross-peak between the H10A and the H10B signal. A distinction between the diastereotopic methyl groups on P3 (proton sets H18 and H19) can be made: methyl group H11 is spatially close to H18, which gives rise to an intense cross-peak between the resonances of these two CH_3 groups. The identified methyl group H18, in turn, shares a cross-peak with methyl group H19.

The further sequencing continues from methyl group H19: it has a second, intense cross-peak, which indicates close proximity, to CH_3 protons assigned as H17 (methyl group bonded to P2, cf. the X-ray structure, Figure 2). The expected cross-peak H17/H16 is hidden in the diagonal, but H16 is easily identified by means of the HMQC spectrum (see below). Methyl group H16, in turn, is close to methyl group H15, which leads to the cross-peak near the diagonal. Of the two diastereotopic protons H7A and H7B, H7A is close to the identified methyl group H15, which leads to the appropriate cross-peak. The H7A resonance is further identified by its cross-peak with methyl group H16. Methyl group H9 has approximately equal distance to protons H7A and H7B, thus the observed cross-peak does not allow one to distinguish between H7A and H7B. Likewise, diastereotopic protons H8A and H8B have equal distance to methyl group H9, which leads to the expected pair of cross-peaks. A distinction between H8A and H8B can be made on the basis of the distances of these two diastereotopic protons from their H7A and H7B counterparts: from the X-ray structure,[7] the distance H7A–H8B is ca. 2.5 Å (cross-peak expected), whereas the corresponding distance H7B–H8A is ca 4.0 Å (no cross-peak expected). Thus, a cross-peak (albeit weak) identifies the "triplet" at δ = 2.345 ppm to be arising from H8B. Trivially, an intense cross-peak is found for the geminal and diastereotopic protons H8B and H8A. An NOE of intermediate strength is found between methyl group H9 and methyl group H14. An NOE of similar strength between methyl group H9 and methyl group H13 is further (and redundant) support of the assignment of H13. Additional redundant NOEs are found between methyl group H14 and the diastereotopic CH_2 proton H7B, between methyl groups H13 and H11 and between methyl groups H14 and H15.

Starting from the assignments of the aliphatic resonance lines of **4**, the assignment of the pyridine signals is straightforward (Figure S4b). The observed correlation between H4

on the pyridine ring and the two sets of methyl hydrogen atoms H11 and H13 attests to the relative rigidity of the structure also in solution. In conclusion, there is complete and unequivocal assignment of all ^{1}H NMR signals of **4**.

Figure 4 shows the ^{31}P,^{1}H HMQC spectrum of **4**, recorded with the delay in the HMQC sequence set for an optimum ^{31}P,^{1}H coupling constant of 14 Hz (Figure 4a) and for 5 Hz (Figure 4b). In Figure 4a, pairs of intense cross-peaks unequivocally identify the ^{31}P resonances of P1, P2 and P3 through their coupling with the methyl group pairs bonded to these phosphorus atoms. In addition, P1 shows cross-peaks occurring as a result of ^2J coupling with protons H7A and H7B, as well as a ^4J coupling with methyl group H9. Similarly, the P2 resonance shows ^2J coupling with H8B; the corresponding coupling with H8A is hidden beneath the intense H16/H17 cross-peaks. In the same way as P1, the P2 resonance exhibits ^4J coupling with methyl group H9. The P3 resonance shows coupling with H10A (H10B cross-peak hidden) and ^4J coupling with methyl group H13 (but not H11), in agreement with the ^{1}H assignments given above.

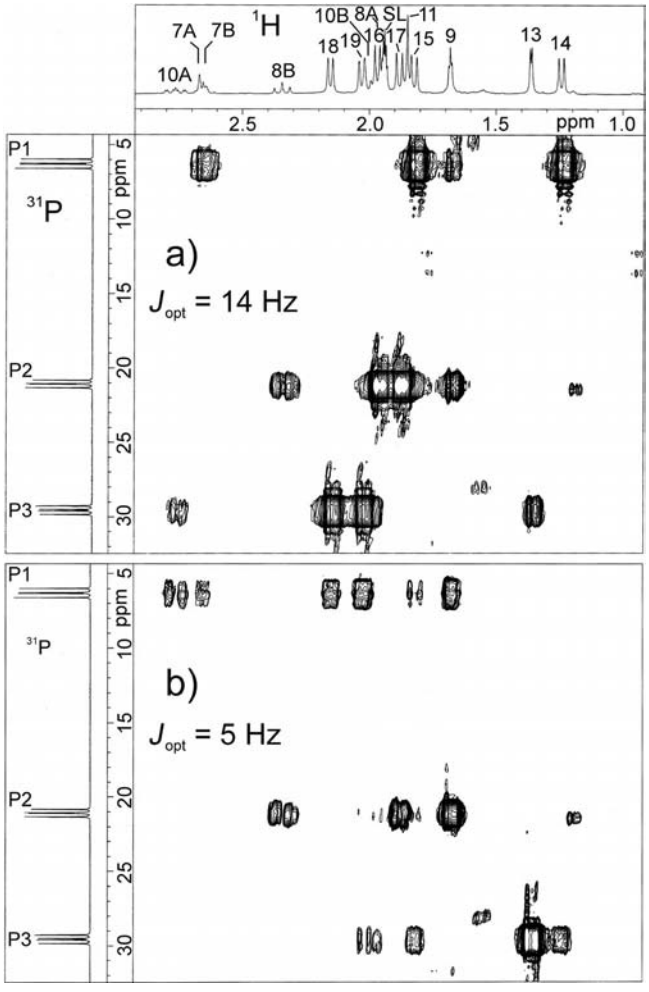

Figure 4. ^{31}P,^{1}H HMQC (pulsed field gradient, magnitude mode) spectrum of **4** (500/202 MHz, CD_3CN, +25 °C). Numbers in the 1D spectra refer to the numbering of the X-ray structure (see Figure 2). SL = solvent signal. (a) Delay in pulse sequence set for $J(P,H)_{opt}$ = 14 Hz. (b) Delay in pulse sequence set for $J(P,H)_{opt}$ = 5 Hz.

Figure 4b is complementary to Figure 4a: here, long-range ^4J couplings are dominant, whereas the larger ^2J couplings are missing or are at least strongly suppressed.

An interesting feature can be found in the ^{1}H resonance line of the diastereotopic protons H7A and H7B. In the ^{31}P-decoupled proton spectrum (Figure 3b), these two protons appear as a strongly coupled AB pattern. However, the ^{31}P-coupled spectrum (Figure 3a) exhibits an "odd" lineshape for these two protons. The underlying reasons are (i) strong coupling between H7A and H7B and (ii) additional coupling with P1, P2 and P3. Thus, we are dealing with an ABXYZ spin system with strong AB coupling. By using the input matrix given in Table 1, a simulation of the resonances H7A and H7B reproduces the experimental data with high accuracy (Figure 5). Note that such spectra cannot be explained on the basis of "first-order rules".

Table 1. Input parameters for the simulation of the ^{1}H signals of H7A and H7B in Figure 5.

Nucleus	Shift	J_{H7A}	J_{H7B}	J_{P1}	J_{P2}
H7A	2.668				
H7B	2.652	15.5			
P1	6.300	4.0	18.0		
P2	21.098	1.0	1.0	56.0	
P3	29.575	0.3	2.8	68.6	48.0

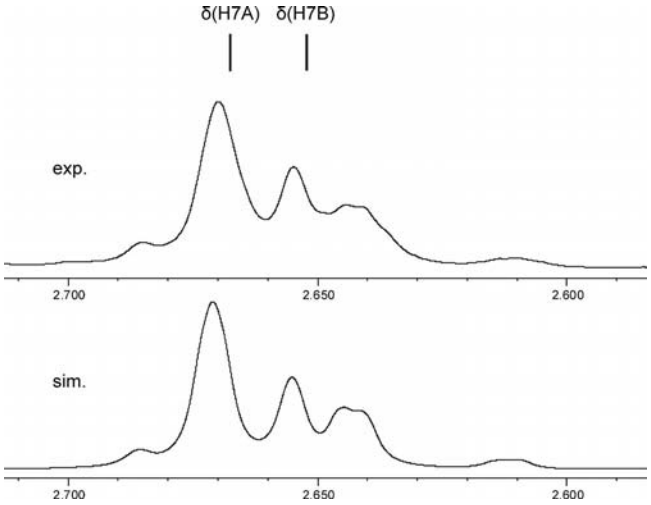

Figure 5. Experimental (above) and simulated (below) ^{1}H signal of H7A and H7B (numbering based on the X-ray structure assignment, Figure 2). The data that have been used for the simulation are given in the Experimental Section and in Table 1. H7A, H7B, P1, P2 and P3 are part of an ABXYZ spectrum, thus explaining the unsymmetric and "odd" shape of the signal. Analysis by using first-order rules fails in this case.

Interestingly, H7A and H7B have completely different coupling constants with respect to the adjacent P1 (4.0 and 18.0 Hz, respectively). The reason for this discrepancy is unknown.

According to the data of Table 1, it should be expected that at least the 2.8 Hz coupling between H7B and P3 should manifest itself as a cross-peak in the HMQC plot of

Figure 4b. In the plot used for illustration, this is not the case. When cutting at a lower level (not shown), this cross-peak is, however, detected.

The assignments of P1, P2 and P3 were further corroborated by a phase-sensitive $^{31}P,^{31}P$ NOESY spectrum (Figure 6). From the X-ray structure,[7] the respective P···P distances are (figures rounded to two significant digits): P1···P2 3.2 Å, P1···P3 4.6 Å, P2···P3 3.4 Å. Thus, in the NOESY spectrum, P1 should have an intense cross-peak with P2 and a weaker cross-peak with P3. The "intermediate" P2 should exhibit equally intense cross-peaks with P1 and P3, and P3 should show an intense cross-peak with P2 and a weaker cross-peak with P1. When examining the f_1 slices shown in Figure 6, these expectations are precisely met.

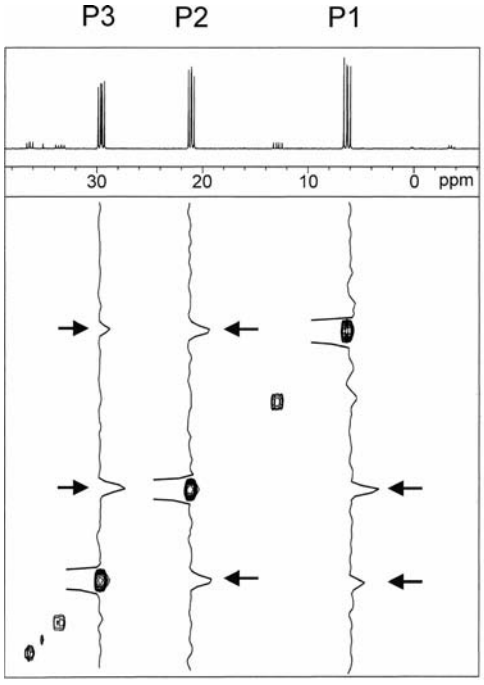

Figure 6. $^{31}P,^{31}P$ NOESY spectrum of **4** (202 MHz, CD_3CN, +25 °C). Numbers P1, P2 and P3 refer to the numbering of the X-ray structure (Figure 2). The vertical insets are f_1 slices taken at the relevant f_2 positions. Note the different cross-peak intensities (arrows) reflecting the different P···P distances. For assignments, see text.

With ^1H decoupling, the three phosphorus atoms in **4** form an AMX spin system under high-field conditions. Thus, the splittings can be analyzed by using simple first-order rules: each resonance line is split into a doublet of a doublet. As a final proof of the correct assignments of the respective P,P coupling constants, a phase-sensitive $^{31}P,^{31}P$ double quantum-filtered COSY spectrum was recorded (Figure 7).

The relevant cross-peak sections show, as is usual for this type of spectra, active couplings as antiphase and passive couplings as in-phase pairs of cross-peaks. The extracted magnitudes of the relevant coupling constants are in agreement with the data extracted from the one-dimensional ^{31}P spectrum (shown in the f_1 dimension in Figure 4). In order

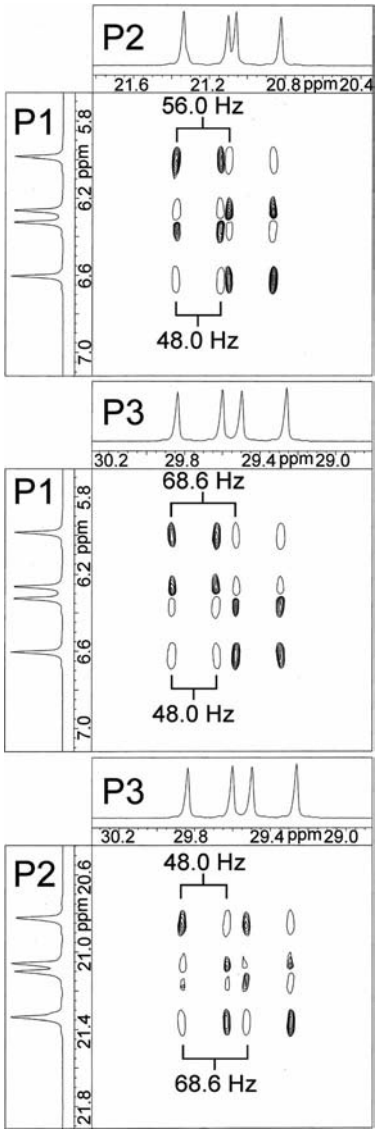

Figure 7. Phase-sensitive $^{31}P,^{31}P$ double quantum filter COSY spectrum of **4**; plots of relevant cross-signals. Positive contours are drawn with more than one level, negative contours are drawn at a single level. Active couplings are antiphase, passive couplings are in-phase.

to conclude the assignment of the ^{31}P signals in **4**, the experimental ^{31}P spectrum has been simulated by using the data given in the Experimental Section and in Table 1 (Figure 8). The experimentally recorded and simulated traces are in excellent agreement. Note that the satellites arising from coupling with ^{57}Fe (I = ½) have been included in the simulation, denoted by asterisks in Figure 8. Interestingly, for all three phosphorus atoms P1, P2 and P3, there is a uniform coupling constant, $^1J(^{31}P,^{57}Fe)$ = 30 Hz.

The NMR study of **4** suggests the solution structure of the dication to be similar to its solid-state structure, particularly with respect to the juxtaposition of the two methyl groups C11 and C13 bonded to the quaternary carbon atom C12. This structure is adopted when two monodentate ligands (2 × CO) combine with the tetradentate NP_3 ligand

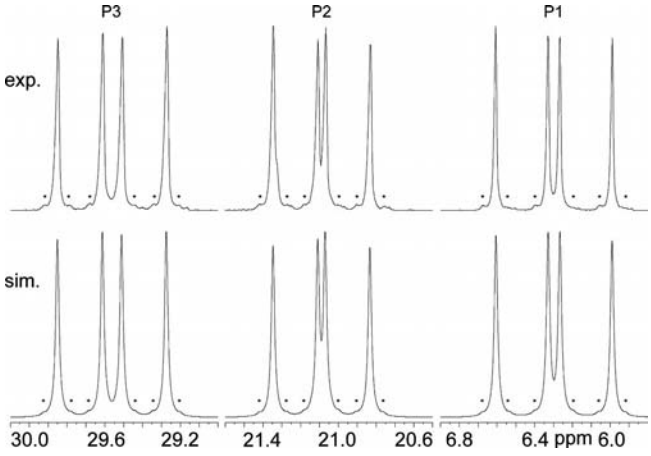

Figure 8. Experimental (above) and simulated (below) ^{31}P signals of **4** (202 MHz, CD_3CN, +25 °C). Labels P1, P2 and P3 refer to the numbering of the X-ray structure (Figure 2). The weak peaks denoted by asterisks are ^{57}Fe satellites.

to complete the coordination octahedron. When there is only one monodentate ligand available, such as diethylphosphane in complex **3**, the NP_3 ligand is sufficiently flexible for one of the methyl groups to come in close contact with the metal centre. The resulting agostic C–H···Fe interaction stabilizes what would otherwise be a vacant coordination site. While the reaction of complex **3** with excess CO produces the *cis*-dicarbonyl complex **4** (and, to a minor extent, the monocarbonyl complex **5**, which contains the NP_4 ligand **1**; see below), the same *cis*-dicarbonyl complex is obtained (as the dibromide salt) upon complexation of the NP_3 ligand **2** with one equivalent of $FeBr_2$ in methanol, followed by exchange of the bromido ligands for CO in a subsequent step (Scheme 4). The dibromido complex **6** may be isolated as a green solid. Its ^1H NMR spectrum provides circumstantial evidence that both Br^- ions are bonded, as bromido ligands, to the metal centre, as there is no high-field signal (around –4 ppm) indicative of a methyl group in agostic interaction with the central metal. It is noteworthy that this complex, of composition $(NP_3)FeBr_2$, is diamagnetic, which suggests strong Fe–P bonding, as has been discussed for a number of complexes of composition $(P_2)_2FeCl_2$, where P_2 denotes a nonbulky, strongly coordinating diphosphane ligand.[23] If only half an equivalent of $FeBr_2$ is used in the complexation reaction, two equivalents of the NP_3 ligand will coordinate the metal centre, which leads to the formation of the *trans*-dibromido complex $[(\mathbf{2})_2FeBr_2]$ (**8**). A small crop of single crystals was obtained, and the coordination of NP_3 as a bidentate ligand through the 1,3-diphosphinopropane sidearm (which is expected to produce a diamagnetic complex, see above) was ascertained by an X-ray structure analysis (Scheme 4). Bond lengths and angles in this structure are unexceptional (see Supporting Information).

In addition to complex **4**, which is the major product, the reaction of **3** with CO, pressurized and in ethanol solution, produces a number of other species. Of these, complex **5** is particularly remarkable for the making of the P–C bond it requires. Complexes **4** and **5** separate from the reaction mixture as a yellow polycrystalline material. The mass spectrum of the remaining mother liquor (ESI; Figure 9) has six prominent signals in the region $350 \leq m/z \leq 550$, all of which are assigned unequivocally on the basis of high-resolution measurements. Two groups of compounds are characterized by a sequential loss of CO. Mass spectra recorded separately of the gas collected in the headspace of the autoclave after reaction show intense signals assigned to diethylphosphane, Et_2PH [which is displaced from iron(II) in the reaction], and diethylphosphane oxide, $Et_2P(=O)H$ (which forms upon aerobic oxidation).

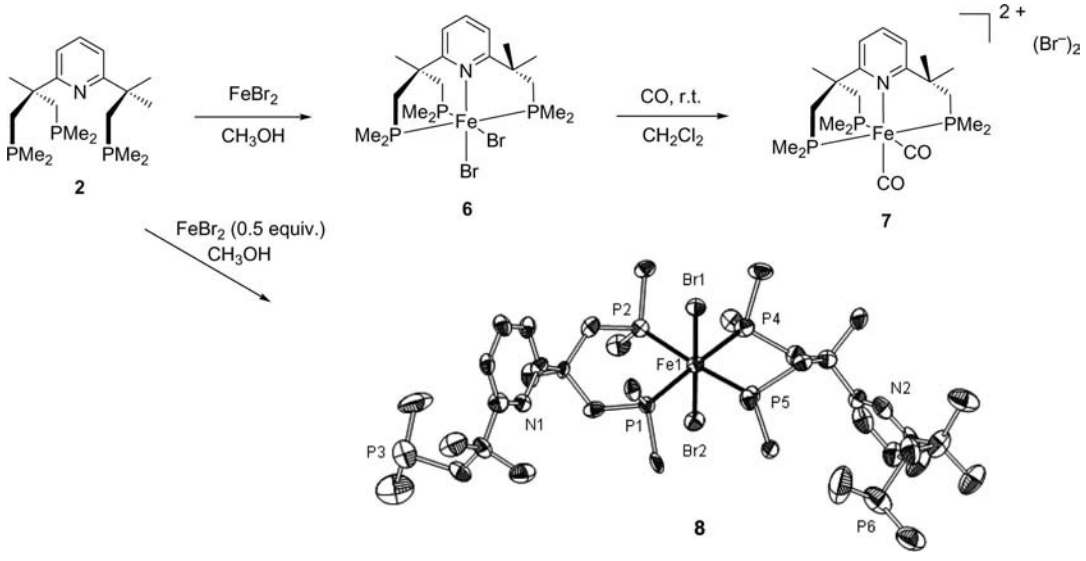

Scheme 4. Formation of the *cis*- and *trans*-dibromido complexes $[(\mathbf{2})FeBr_2]$ (**6**) and $[(\mathbf{2})_2FeBr_2]$ (**8**), respectively, depending on the stoichiometry of reactants. The dicarbonyl complex **7** may be prepared from **6** by Br^-/CO exchange.

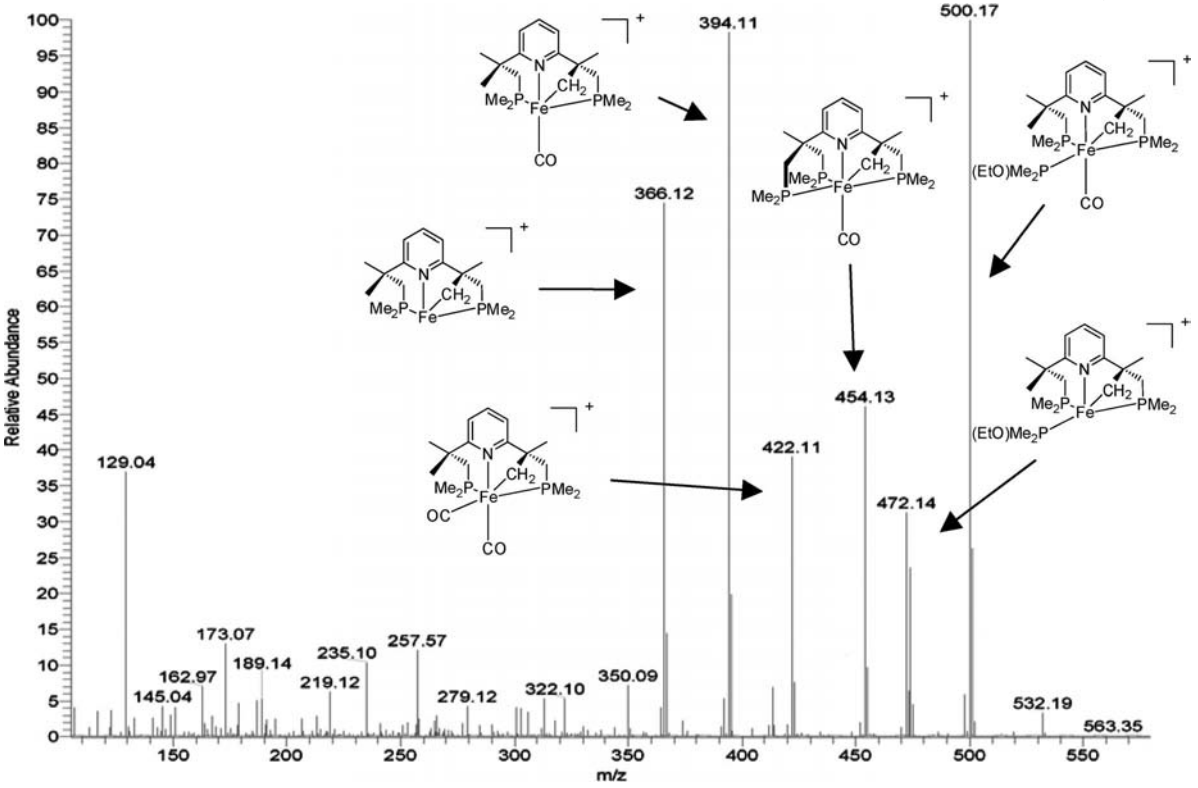

Figure 9. ESI spectrum of the mother liquor of the reaction of complex **3** with CO (autoclave, ethanol solution).

On the basis of the products identified in the mother liquor, we suggest the following sequence of reactions leading, inter alia, to the formation of complex **5** (Scheme 5; complexes **4** and **5** are formed in a ratio of approximately 40:1): Both the diethylphosphane ligand and the "agostic" methyl group in **3** are displaced by CO to give the *cis*-dicarbonyl complex **4** as the major product. In what appears to be a side reaction, complex **3** can also be transformed into complex **9**, which resembles somewhat the P–C bond activation product obtained from the reaction of the original NP_4 ligand, Fe^{2+} and the nucleophilic alcohol solvent.[6] In **3**, with concomitant deprotonation of the agostic methyl group, the diethylphosphane ligand is oxidized to ethyl diethylphosphinite (prominent signals for the latter in both mother liquor and headspace). This latter reaction amounts to the formal displacement of dihydrogen ($H^+ + H^-$), which may be driven by the formation of formaldehyde from CO and H_2. Complex **9** may undergo the same type of P–C bond scission to give complex **10**, which has an NP_2 ligand coordinated to iron(II), in addition to ethyl dimethylphosphinite [$Me_2P(OEt)$] and CO. Protonation of the NP_2 residue and formation of the NP_2 ligand $C_5H_3N[CMe_2(CH_2PMe_2)]_2$ has been observed previously.[7] We postulate the carbanionic RCH_2^- residue in complex **9** to be sufficiently electron-releasing/nucleophilic for two equivalents of this complex to undergo a dissymetrization reaction, as shown in Scheme 5, with concomitant transfer of what formally is a dimethyl phosphenium moiety (Me_2P^+) between the two equivalents of complex. This reactivity resembles the mechanism invoked to rationalize the transfer of a dimethylphosphanyl residue to a metal-coordinated nucleophilic alkoxide, RO^- (R = Me, Et), in the original P–C bond cleavage reaction involving the NP_4 ligand **1**.[6,17,18] From two equivalents of complex **9**, the reaction can thus produce one equivalent of complex **5**, which contains the tetrapodal pentadentate NP_4 ligand, and one equivalent of complex **11**, which is different from complex **10** only in that it is a dicarbonyl species instead of having one monodentate P ligand. The presence of the strongly electron-releasing donor RCH_2^- in **9** may favour the formation of complex **11**, which contains the two strongly π-acidic CO ligands, in this dissymetrization reaction. We are, however, not aware of a previous example of formal R_2P^+ transfer to a carbanion in the coordination sphere of a transition metal.[19] The observed reactivity suggests that the mother liquor of the reaction, when reacted anew with CO under pressure, should yield more of the NP_4 complex **5**, which has been shown to be the case in a separate experiment.

Conclusions

This study describes the reactivity of a pyridine-derived triphosphane ligand coordinated to iron(II), in the presence of nucleophilic alcohol solvent and carbon monoxide. Both P–C bond scission and formation are observed, depending on the species participating in the reaction, with formal transfer of a phosphenium moiety (Me_2P^+) in both cases. The PMe_2 residue, as part of what initially is the intact che-

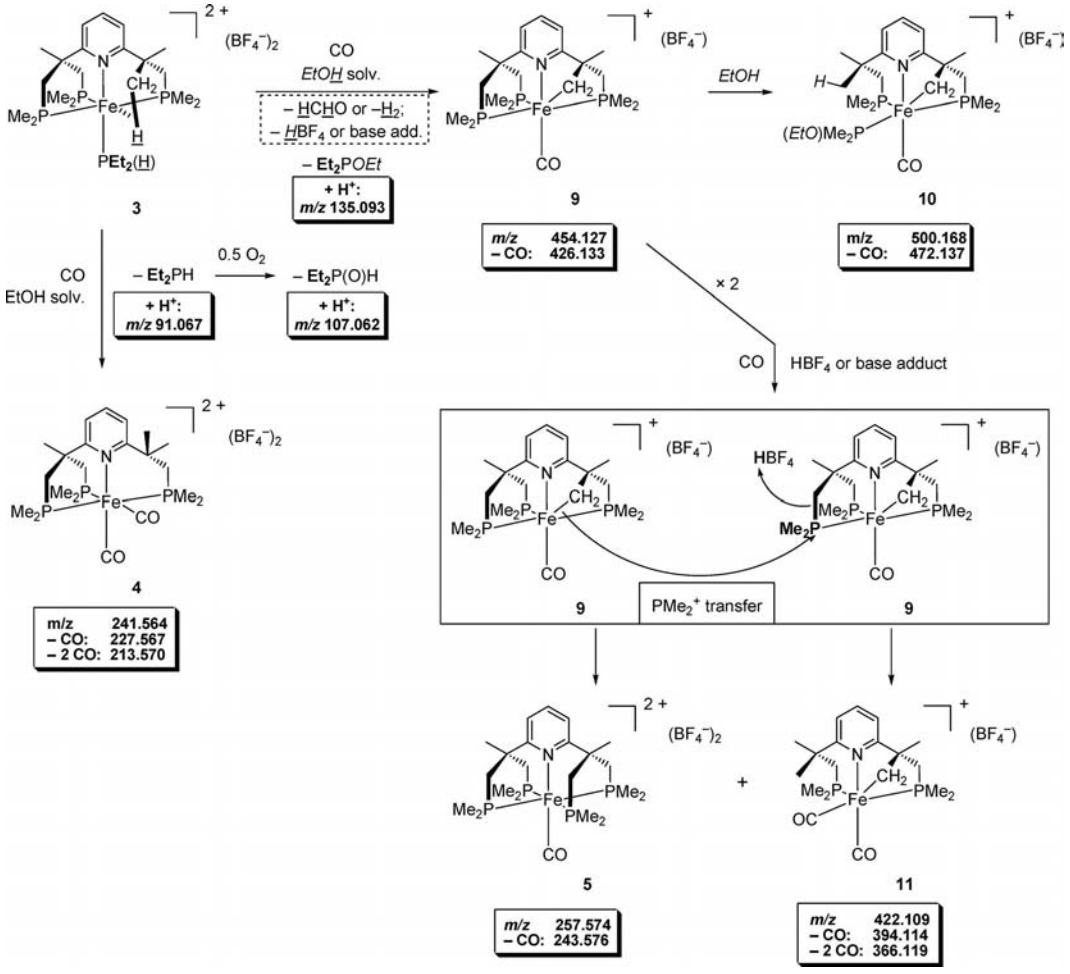

Scheme 5. Suggested sequence of reactions explaining the formation of complexes **5**, **9**, **10** and **11** (the stereochemistry of some complexes is uncertain). Two equivalents of **9** are postulated to undergo exchange of a phosphenium moiety (PMe_2^+). In addition to **5**, the dissymmetrization reaction generates one equivalent of complex **11**. All parent ions have prominent signals (*m*/*z* values shown in boxes) in the ESI mass spectra.

late ligand, appears to become increasingly susceptible to nucleophilic attack with an increasing number of CO ligands (i.e. π acids) in the coordination sphere of iron(II). Both P–O and P–C bonds are thus formed (giving phosphinite and phosphane moieties, respectively), depending on the reaction conditions. As a reference for future work aimed at putting the observed reactivity to synthetic use, one of the complexes was analyzed fully by using a combination of NMR spectroscopic techniques.

Experimental Section

Materials and Instrumentation: Unless noted otherwise, all reactions were carried out at room temperature in dried solvents under dry dinitrogen by using standard Schlenk techniques. Diethylphosphane was prepared in either of two ways: chlorodiethylphosphane was reduced to diethylphosphane by using $LiAlH_4$ in diethyl ether at –78 °C (81% yield)[7,11] or tetraethyldiphosphane disulfide was generated from thiophosphoryl chloride by reaction with ethylmagnesium bromide (THF, –2 °C), followed by reduction with $LiAlH_4$ in diethyl ether.[7,12,13] $Fe(BF_4)_2{\cdot}6H_2O$ was purchased from Aldrich and used without further purification. Carbon monoxide (99.997%) was purchased from Air Liquide. IR spectra of solids were measured on KBr discs and assigned on the basis of literature data.[20] The following instruments were used for spectroscopic measurements: IR spectroscopy, Nicolet Magna System 750; mass spectrometry, Varian 311 A and Spektrospin CMS FT-ICR; NMR spectroscopy, Bruker ARX 200 and Bruker ARX 400. ^1H and ^{31}P NMR spectra of **4**: JEOL Alpha500 spectrometer (^1H: 500 MHz; ^{31}P: 202 MHz). An inverse 5-mm probe head with actively shielded gradient coils was employed, with the exception for the $^{31}P,^{31}P$ NOESY spectrum shown in Figure 6 (normal 5-mm broadband probe head). Labels refer to the labelling of the X-ray structure (Figure 2). ^1H NMR spectra are referenced to the residual solvent signals of methanol and acetonitrile (δ = 1.94 ppm). ^{31}P NMR spectra were referenced to 80% H_3PO_4 by using the substitution method.[21] No corrections for different bulk magnetic susceptibilities were made; simulations of spectra were carried out with the software package "gNMR" by P. Budzelaar[22], Version 5.0.6.0, IvorySoft, formerly distributed by Adept Scientific. The chemical shifts and coupling constants used for the simulation fits in Figures 5 and 8 were adjusted manually instead of using the built-in iteration routine. The $^{31}P,^{57}Fe$ coupling constant was set to 30.0 Hz for all three phosphorus atoms P1, P2 and P3. Relative signs of all coupling constants employed in Figures 5 and 8 are positive throughout. For the higher-order spectrum of Figure 5, a change in the relative signs of the $^{31}P,^1H$ coupling constants leads to dramatic

spectral changes, the relative signs are thus considered correct. For the first-order ^{31}P spectrum in Figure 8, a change in the relative signs of the $^{31}P,^{31}P$ coupling constants has no spectral effect at all. The true signs are unknown. Elemental analyses were carried out with a Thermo Finnigan, Flash EA, 1112 Series analyzer.

[Fe(2)(Et$_2$PH)](BF$_4$)$_2$ (3): Diethylphosphane (70 mg, 0.78 mmol, 0.09 mL) was added to a solution of **2** (290 mg, 0.781 mmol) in ethanol (3 mL), and the mixture stirred for 10 min. A solution of $Fe(BF_4)_2{\cdot}6H_2O$ (194 mg, 0.586 mmol, 0.75 equiv.) in ethanol (3 mL) was added dropwise. A purple solid began to precipitate, and the suspension was allowed to stir for 45 min. The precipitate was then filtered, washed with ethanol (3 × 2 mL) and diethyl ether (3 × 2 mL) and dried in vacuo to yield purple microcrystals (243 mg, 0.352 mmol, 60%). ^{1}H NMR (200 MHz, [D$_4$]methanol, r.t.): δ = 8.13 [t, ^3J(H,H) = 8.3 Hz, 1 H, py-H^{para}], 7.86 [d, ^3J(H,H) = 7.9 Hz, 1 H, py-H^{meta}], 7.65 [d, ^3J(H,H) = 7.6 Hz, 1 H, py-H^{meta}], 4.70 [d, ^1J(P,H) = 332 Hz, 1 H, P*H*], 2.55, 2.48 (m/m, 2 H, CH_2), 2.32–2.01 (br., 4 H, 2 × CH_2), 2.01–1.82 (m, 6 H, 2 × PCH_3), 1.84 (s, 6 H, 2 × CCH_3), 1.68–1.57 (br., 4 H, 2 × PCH_2CH$_3$), 1.39 [t, ^3J(H,H) = 10.0 Hz, 6 H, 2 × PCH$_2$CH_3], 1.34–1.25 (m, 6 H, 2 × PCH_3), 0.91–0.74 (m, 6 H, 2 × PCH_3), –3.73 (s, 3 H, CH_3) ppm. ^{31}P NMR (80.95 MHz, [D$_4$]methanol, r.t.): δ = 47.59 (m, *P*Me$_2$), 40.14 [m, ^1J(P,H) = 332 Hz, Et$_2$*P*H], 23.59 (m, *P*Me$_2$), 18.92 (m, *P*Me$_2$) ppm. ^{13}C NMR (160.64 MHz, [D$_4$]methanol, r.t.): δ = 170.87 (s, py-C^{ortho}), 169.12 (s, py-C^{ortho}), 142.46 (s, py-C^{para}), 124.43 (s, py-C^{meta}), 123.99 (s, py-C^{meta}), 45.41 (s, *C*CH$_3$), 44.30 (s, *C*CH$_3$), 43.45 (m, *C*H$_2$), 38.04 (m, *C*H$_2$), 37.83 (m, *C*H$_2$), 32.20 (m, P*C*H$_2$CH$_3$), 29.88 (m, P*C*H$_2$CH$_3$), 28.52 (m, C*C*H$_3$), 26.64 (m, C*C*H$_3$), 24.66 (m, C*C*H$_3$), 21.17 (m, P*C*H$_3$), 18.74 (m, P*C*H$_3$), 18.48 (m, P*C*H$_3$), 16.64 (m, P*C*H$_3$), 16.01 (m, P*C*H$_3$), 13.58 (m, P*C*H$_3$), 12.28 (m, PCH$_2$*C*H$_3$), 12.22 (m, PCH$_2$*C*H$_3$) ppm. $C_{23}H_{47}B_2F_8FeNP_4$ (690.97 g/mol): calcd. C 39.98, H 6.86, N 2.03; found C 40.05, H 6.44, N 1.94.

[Fe(2)(CO)$_2$](BF$_4$)$_2$ (4) and [Fe(1)CO](BF$_4$)$_2$ (5): A suspension of **3** (125 mg, 0.181 mmol) in ethanol (8 mL) was treated with CO (10 bar) in an autoclave at 65 °C for 4 h. During the reaction, the colour of the solid changed from purple to yellow. The suspension was transferred to an empty flask, and the solution removed by syringe. The remaining yellow solid was washed with diethyl ether (2 × 3 mL) and dried in vacuo (105 mg). Subsequent analysis showed it to be a mixture of compounds **4** and **5** in a ratio of approximately 40:1 [the yields of **4** and **5** with respect to the amount of **3** employed in the reaction are thus approximately 0.156 mmol or 86% (**4**) and 0.004 mmol or 2% (**5**)]. Isothermal diffusion of diethyl ether into a solution of the material in acetonitrile gave a small crop of single crystals of **4**.

Data for compound **4**: ^{1}H NMR (500 MHz, [D$_3$]acetonitrile, r.t.): δ = 8.01 [dd, ^3J(H,H) = 7.9, ^3J(H,H) = 7.9 Hz, 1 H, H3], 7.92 [d, ^3J(H,H) = 7.9 Hz, 1 H, H4], 7.84 [d, ^3J(H,H) = 7.9 Hz, 1 H, H2], 2.77 [ddd, ^2J(H10A,H10B) = 15.6, ^2J(H10A,P3) = 17.7, ^4J(H10A,P1) = 4.3 Hz, 1 H, H10A], 2.67 [non-first-order multiplet, ^2J(H7A,H7B) = 15.5, ^2J(H7A,P1) = 4.0, ^4J(H7A,P2) = 1.0, ^4J(H7A,P3) = 0.3 Hz, 1 H, H7A], 2.65 [non-first-order multiplet, ^2J(H7B,H7A) = 15.5, ^2J(H7B,P1) = 18.0, ^4J(H7B,P2) = 1.0, ^4J(H7B,P3) = 2.8 Hz, 1 H, H7B], 2.34 [dd, ^2J(H8B,H8A) = 15.3, ^2J(H8B,P2) = 15.3 Hz, 1 H, H8B], 2.15 [d, ^2J(H18,P3) = 9.5 Hz, 3 H, H18], 2.03 [dd, ^2J(H19,P3) = 10.7, ^4J(H19,P1) = 1.5 Hz, 3 H, H19], 2.00 [d, ^2J(H10B,H10A) = 15.6 Hz, 1 H, H10B], 1.98 [d, ^2J(H8A,H8B) = 15.3 Hz, 1 H, H8A], 1.97 [d, ^2J(H16,P2) = 9.8 Hz, 3 H, H16], 1.88 [d, ^2J(H17,P2) = 11.0 Hz, 3 H, H17], 1.85 (s, 3 H, H11), 1.82 [dd, ^2J(H15,P1) = 10.4, ^4J(H15,P3) = 0.9 Hz, 3 H, H15], 1.68 [dd, ^4J(H9,P1) = ^4J(H9,P2) = 3.1 Hz, 3 H, H9], 1.36 [d, ^4J(H13,P3) = 3.4 Hz, 3 H, H13], 1.24 [dd, ^2J(H14,P1) = 9.8, ^4J(H14,P2) = 0.9 Hz, 3 H, H14] ppm. ^{31}P{^{1}H} NMR (202 MHz, [D$_3$]acetonitrile, r.t.): δ = 29.57 (dd, *J* = 48.0 Hz, 68.6 Hz, P3), 21.10 (dd, *J* = 56.0 Hz, 48.0 Hz, P2), 6.30 (dd, *J* = 56.0 Hz, 68.6 Hz, P1) ppm. ^{13}C NMR (100.64 MHz, [D$_3$]acetonitrile, r.t.): δ = 207.99 (m, *C*O), 206.13 (m, *C*O), 180.27 (s, py-C^{ortho}), 172.82 (s, py-C^{ortho}), 140.91 (s, py-C^{para}), 125.82 (s, py-C^{meta}), 124.70 (s, py-C^{meta}), 45.15 (s, *C*CH$_3$), 44.34 (s, *C*CH$_3$), 38.10 (m, *C*H$_2$), 37.32 (m, *C*H$_2$), 36.43 (m, *C*H$_2$), 35.35 (m, C*C*H$_3$), 32.10 (m, C*C*H$_3$), 29.68 (m, C*C*H$_3$), 21.04 (m, P*C*H$_3$), 19.12 (m, P*C*H$_3$), 18.90 (m, P*C*H$_3$), 18.50 (m, P*C*H$_3$), 17.38 (m, P*C*H$_3$), 14.47 (m, P*C*H$_3$) ppm. IR (KBr): $\tilde{\nu}$ = 2060 (vs, CO), 2015 (vs, CO), 1083 (vs, BF_4^-) cm^{-1}. ESI-MS: *m*/*z* (%) = 241.564 (25) $[M]^{2+}$, 227.567 (42) $[M - CO]^{2+}$, 213.570 (100) $[M - 2\ CO]^{2+}$. $C_{21}H_{36}B_2F_8FeNO_2P_3$ (656.89): calcd. C 38.40, H 5.52, N 2.13; found C 38.76, H 5.65, N 2.09.

Data for compound **5**: ^{1}H NMR (400 MHz, [D$_3$]acetonitrile, r.t.): δ = 7.72 (br., 1 H, py-H^{para}), 8.08 (br., 2 H, py-H^{meta}), 2.59–2.40 (br., 8 H, CH_2), 1.63–1.50 (br., 24 H, PCH_3), 1.47 (s, 6 H, CCH_3) ppm. ^{31}P NMR (161.97 MHz, [D$_3$]acetonitrile, r.t.): δ = 19.26 (s, 4 × *P*Me$_2$) ppm. ^{13}C NMR (100.64 MHz, [D$_3$]acetonitrile, r.t.): δ = 207. 85 (m, 1 C, *C*O), 168.35 (s, 2 C, py-2 × C^{ortho}), 142.16 (s, 2 C, 2 × py-C^{meta}), 126.43 (s, 1 C, 2 × py-C^{para}), 45.74 (s, 2 C, 2 × *C*CH$_3$), 44.00 (s, 4 C, 4 × *C*H$_2$), 34.76 (s, 2 C, 2 × C*C*H$_3$), 18.15 (m, 8 C, 8 × P*C*H$_3$) ppm. ESI-MS: *m*/*z* (%) = 257.573 (5) $[M]^{2+}$, 227.567 (4) $[M - CO]^{2+}$. $C_{22}H_{41}B_2F_8FeNOP_4$ (688.92): calcd. C 38.36, H 6.00, N 2.03; found C 38.76, H 5.65, N 2.09.

[Fe(2)Br$_2$] (6): A solution of $FeBr_2$ (182 mg, 0.844 mmol) in methanol (3 mL) was added to a solution of **2** (330 mg, 0.880 mmol) in methanol (10 mL). The colour of the solution changed to dark green. The mixture was left to stir overnight, after which time a light green solid precipitated. The solid was filtered and dried in vacuo to yield a light green powder (342 mg, 0.582 mmol, 69%). ^{1}H NMR (200 MHz, [D$_2$]dichloromethane, r.t.): δ = 7.94 (br., 1 H, py-H^{para}), 7.88 (br., 1 H, py-H^{meta}), 7.84 (br., 1 H, py-H^{meta}), 2.32 (br., 6 H, CH_2), 1.88 (s, 3 H, CH_3), 1.77 (br., 3 H, CH_3), 1.36 (br., 3 H, CH_3), 1.05 (br., 9 H, PCH_3), 0.75 (br., 9 H, PCH_3) ppm, no signal in the negative ppm range. ^{31}P{^{1}H} NMR (80.95 MHz, [D$_2$]-dichloromethane, r.t.): δ = 50.14 (m, 1 P, *P*Me$_2$), 27.57 (m, 1 P, *P*Me$_2$), 16.51 (m, 1 P, *P*Me$_2$) ppm. IR (KBr): $\tilde{\nu}$ = 372 (s, Fe–Br), 352 (s, Fe–Br) cm^{-1}.

[Fe(2)(CO)$_2$]Br$_2$ (7): CO was passed into a solution of **6** (150 mg, 0.255 mmol) in dichloromethane (5 mL) for 3 min. The mixture was left to stir overnight under CO atmosphere, after which time the colour of the solution changed from green to orange. The solvent was removed by distillation to yield an orange solid. ^{1}H NMR (200 MHz, [D$_2$]dichloromethane, r.t.): δ = 7.98 [dd, ^3J(H,H) = 7.8, ^3J(H,H) = 7.8 Hz, 1 H, H3], 7.90 [d, ^3J(H,H) = 7.8 Hz, 1 H, H4], 7.81 [d, ^3J(H,H) = 7.8 Hz, 1 H, H2], 2.79 (m, 1 H, H10A), 2.70 (1 H, H7A), 2.65 (m, 1 H, H7B), 2.32 (m, 1 H, H8B), 2.18 (br., 3 H, H18), 2.03 (br., 3 H, H19), 1.98 (br., 1 H, H10B), 1.98 (br., 1 H, H8A), 1.94 [d, ^2J(H16,P2) = 9.8 Hz, 3 H, H16], 1.86 [d, ^2J(H17,P2) = 11.0 Hz, 3 H, H17], 1.80 (s, 3 H, H11), 1.79 (m, 3 H, H15), 1.67 (m, 3 H, H9), 1.33 [d, ^4J(H13,P3) = 3.3 Hz, 3 H, H13], 1.19 (m, 3 H, H14) ppm. ^{31}P{^{1}H} NMR (80.95 MHz, [D$_2$]dichloromethane, r.t.): δ = 29.77 (dd, *J* = 49.0 Hz, 68.8 Hz, P3), 22.10 (dd, *J* = 55.0 Hz, 48.5 Hz, P2), 6.35 (dd, *J* = 57.2 Hz, 68.7 Hz, P1) ppm. ^{13}C NMR (50.32 MHz, [D$_2$]dichloromethane, r.t.): δ = 215.97 (m, *C*O), 213.13 (m, *C*O), 180.87 (s, py-C^{ortho}), 173.42 (s, py-C^{ortho}), 139.89 (s, py-C^{para}), 125.45 (s, py-C^{meta}), 123.70 (s, py-C^{meta}), 45.77 (s, *C*CH$_3$), 44.39 (s, *C*CH$_3$), 37.90 (m, *C*H$_2$), 38.30 (m, *C*H$_2$), 35.44 (m, *C*H$_2$), 35.39 (m, C*C*H$_3$), 31.90 (m, C*C*H$_3$), 30.01 (m, C*C*H$_3$), 20.14 (m, P*C*H$_3$), 19.52 (m, P*C*H$_3$), 18.94 (m, P*C*H$_3$), 18.62 (m,

PCH_3), 17.10 (m, PCH_3), 14.50 (m, PCH_3) ppm. IR (KBr): $\tilde{\nu}$ = 1962 (vs, CO), 1927 (vs, CO) cm^{-1}.

[Fe(2)$_2$Br$_2$] (8): A solution of $FeBr_2$ (90 mg, 0.418 mmol, 0.5 equiv.) in methanol (3 mL) was added to a solution of **2** (315 mg, 0.840 mmol) in methanol (5 mL). The solution changed its colour to green and was left to stir overnight. Isothermal diffusion of diethyl ether into the solution gave a small crop of single crystals of **8**. Crystal-structure determination: X-ray diffraction intensity data for **8** was collected on an Oxford Diffraction Xcalibur S Sapphire diffractometer. The structure was solved by direct methods (SHELXS-97). All non-hydrogen atoms were refined anisotropically. Bond lengths and angles, as well as crystallographic data are given in the Supporting Information. CCDC-791001 (**8**) contains the supplementary crystallographic data for this paper. These data can be obtained free of charge from the Cambridge Crystallographic Data Centre via www.ccdc.cam.ac.uk/data_request/cif.

Supporting Information (see footnote on the first page of this article): Scheme describing the synthesis of the triphosphane **2**; ^{31}P-coupled ^{1}H NMR spectrum and ^{1}H-coupled ^{31}P NMR spectrum of **3**, ^{31}P NMR spectrum and IR spectrum (detail) of the reaction mixture containing complexes **4** and **5**, ^{1}H,^{1}H NOESY spectrum (phase-sensitive) of **4**, table of bond lengths and angles in **8** and selected crystallographic data for **8** are presented.

Acknowledgments

Support of this research by the Deutsche Forschungsgemeinschaft is gratefully acknowledged. We thank Dr. M. Schlangen for measurement of the mass spectra.

[1] A. Grohmann, *Dalton Trans.* **2010**, *39*, 1432–1440.
[2] J. Pitarch López, F. W. Heinemann, R. Prakash, B. A. Hess, O. Horner, C. Jeandey, J.-L. Oddou, J.-M. Latour, A. Grohmann, *Chem. Eur. J.* **2002**, *8*, 5709–5722.
[3] M. Schlangen, J. Neugebauer, M. Reiher, D. Schröder, J. Pitarch López, M. Haryono, F. W. Heinemann, A. Grohmann, H. Schwarz, *J. Am. Chem. Soc.* **2008**, *130*, 4285–4294.
[4] J. P. Boyd, M. Schlangen, A. Grohmann, H. Schwarz, *Helv. Chim. Acta* **2008**, *91*, 1430–1434.
[5] H. I. Karunadasa, C. J. Chang, J. R. Long, *Nature* **2010**, *464*, 1329–1333.
[6] S. W. Kohl, F. W. Heinemann, M. Hummert, W. Bauer, A. Grohmann, *Chem. Eur. J.* **2006**, *12*, 4313–4320.
[7] S.-A. Gentschow, S. W. Kohl, F. W. Heinemann, W. Bauer, D. Wiedemann, A. Grohmann, *Z. Naturforsch., Teil B* **2010**, *65*, 238–250.
[8] J. Ruiz, S. García-Granda, M. R. Díaz, R. Quesada, *Dalton Trans.* **2006**, 4371–4376.
[9] A. Acosta-Ramírez, M. Flores-Álamo, W. D. Jones, J. J. García, *Organometallics* **2008**, *27*, 1834–1840.
[10] N. P. Mankad, M. T. Whited, J. C. Peters, *Angew. Chem. Int. Ed.* **2007**, *46*, 5768–5771.
[11] H. H. Karsch, A. Appelt, *Z. Naturforsch., Teil B* **1983**, *38*, 1399–1405.
[12] K. Issleib, A. Tzschach, *Chem. Ber.* **1959**, *92*, 704–711.
[13] G. W. Parshall, A. H. Cowley, L. F. Centofanti, *Inorg. Synth.* **1968**, *11*, 157–159.
[14] G. Reichenbach, G. Cardaci, G. Bellachioma, *J. Chem. Soc., Dalton Trans.* **1982**, 847–850.
[15] N. Meyer, A. J. Lough, R. H. Morris, *Chem. Eur. J.* **2009**, *15*, 5605–5610.
[16] C. E. Zachmanoglou, A. Docrat, B. M. Bridgewater, G. Parkin, C. G. Brandow, J. E. Bercaw, C. N. Jardine, M. Lyall, J. C. Green, J. B. Keister, *J. Am. Chem. Soc.* **2002**, *124*, 9525–9546.
[17] S. W. Kohl, F. W. Heinemann, M. Hummert, W. Bauer, A. Grohmann, *Dalton Trans.* **2006**, 5583–5592.
[18] S. W. Kohl, F. W. Heinemann, M. Hummert, H. Weißhoff, A. Grohmann, *Eur. J. Inorg. Chem.* **2006**, 3901–3910.
[19] S. A. Macgregor, T. Wondimagegn, *Organometallics* **2007**, *26*, 1143–1149.
[20] G. Socrates, *Infrared Characteristic Group Frequencies*, Wiley, New York, **1994**.
[21] R. K. Harris, E. D. Becker, S. M. Cabral de Menezes, R. Goodfellow, P. Granger, *Pure Appl. Chem.* **2001**, *73*, 1795–1818.
[22] P. H. M. Budzelaar, *gNMR, Version 5.0.6.0*, IvorySoft, Nijmegen, **2006**.
[23] M. V. Baker, L. D. Field, T. W. Hambley, *Inorg. Chem.* **1988**, *27*, 2872–2876.

Received: September 23, 2010
Published Online: December 22, 2010

